Research Article Adv. Mater. Lett. 2016, **7**(1), 29-35 Advanced Materials *Letters*

www.amlett.com, www.vbripress.com/aml, DOI: 10.5185/amlett.2016.6001 Published online by the VBRI Press in 2016

Study the influence of different mol% BLTMNZ doping on KNLN ceramics by using the XRD and impedance spectroscopy

Shweta Thakur[1], Radheshyam Rai[1*], Seema Sharma[2] and Ashutosh Tiwari[3, 4]

[1]*School of Physics, Shoolini University, Solan 173229, Himachal Pradesh, India*
[2]*Ferroelectric Research Laboratory, Department of Physics, A. N. College, Patna 800013, India*
[3]*Biosensors and Bioelectronics Centre, IFM, Linkoping University, Linkoping 58183, Sweden*
[4]*Tekidag AB, UCS, Teknikringen 4A, Mjärdevi Science Park, Linköping 583 30, Sweden*

[*]Corresponding author. E-mail: rshyam1273@gmail.com

Received: 23 May 2015, Revised: 17 November 2015 and Accepted: 05 December 2015

ABSTRACT

Polycrystalline samples of $(K_{0.45}Na_{0.45}Li_{0.1}NbO_3)_{1-x}$-$(Ba_{0.96}La_{0.04}Ti_{0.815}Mn_{0.0025}\ Nb_{0.0025}Zr_{0.18}\ O_3)_x$ ceramics (where x = 0.1, 0.3, 0.5, 0.7 and 0.9) were prepared by using a high temperature solid state reaction technique. The XRD patterns of the BLTMNZ doped KNLN at room temperature with x = 0.7 have pure pervoskite phase with tetragonal structure at room temperature and have maximum value of dielectric constant at x = 0.9. Detailed studies of dielectric and impedance properties of the materials in a wide range of frequency (100Hz–1MHz) and temperatures (30 – 500 ^{0}C) showed that properties are strongly temperature and frequency dependent. The plots of Z″ and M″ versus frequency at various temperatures show peaks in the higher temperature range (>300 ^{0}C). The compounds show dielectric relaxation, which is found to be of non-Debye type and the relaxation frequency shifted to higher side with increase in temperature. The Nyquist plot and conductivity studies showed the NTCR character of samples. Copyright © 2016 VBRI Press.

Keywords: X-ray diffraction; structural; dielectric; electrical properties; impedance spectroscopy.

Introduction

PZT-based ceramics contain up to 60 wt% of lead **[1]**, which has impacts on the human health and the environment. Due to this high toxicity of PbO and its high vapour pressure during processing have stimulated an increasing demand for environment-friendly materials. Research on lead-free piezoelectric materials is mainly focused on alkali niobates and modified bismuth titernates **[2, 3]**. $K_{0.5}Na_{0.5}NbO_3$ (KNN) based ceramics, showing greater advantages over other lead-free piezoelectric systems, attract much attention of researchers for their high Curie temperature and enhanced piezoelectric response **[4-6]**. Potassium sodium niobate KNN has been well known as one of the top-class lead-free piezoelectric materials. Shirane *et al.* made the first systematic structural and dielectric investigation on KNN ceramics with the help of X-ray and Dielectric measurements in 1954 **[7]**. Piezoelectricity of KNN was first studied by Egerton and Dillon, and they found that the radial coupling coefficient of KNN is excellent. However, pure KNN ceramics has low piezoelectric activity due to its poor densification induced by high volatilization of potassium during sintering. In order to enhance its densification behaviour and piezoelectric activity, Li, Ta and Sb are added into the KNN compositions to form new solid solutions **[8, 9]**. Pure KNN have two dielectric peaks at around 200 °C and 400 °C which correspond to phase transition from orthorhombic to tetragonal (T_{O-T}) and from tetragonal to cubic symmetry (T_{T-C}) **[4]**. $(1-x)(K_{0.48}Na_{0.52})NbO_3$-$x(Bi_{0.5}(Na_{0.7}K_{0.2}Li_{0.1})_{0.5}ZrO_3$ (x = 0-0.7) the ceramics with x = 0 and 0.04 have two phase transitions above room temperature, which are assigned to the coexistence of orthorhombic to tetragonal phases (T_{O-T}) and the tetragonal to cubic phases (T_{T-C}). The addition of BNKLZ results in a denser microstructure with a larger grain size **[10, 11]**. Jong-Ho Park *at el.* have reported that the ferroelectric phase transition of NKN-LNx ($x \leq 0.1$), is a second-order transition without thermal hysteresis, and NKN-LNx ($x \geq 0.2$) is a weak first-order transition with small thermal hysteresis **[12]**.

Barium titanate ($BaTiO_3$) is the most common ferroelectric material, which is used as a capacitor, ferroelectric memory because of its excellent dielectric and ferroelectric properties **[13]**. The dielectric properties of barium titanate can be modified by the addition of the dopants such as La^{3+}, Mn^{4+}, Nb^{5+}, and Zr^{4+} to occupy Ba^{2+} on A sites or Ti^{4+} on B sites to form the solid solution **[14-16]**. The effects of Nb_2O_5 addition on the dielectric properties and phase formation of $BaTiO_3$ were investigated by Y. Yuan *at el.* and found that the first dielectric constant peak at curie temperature was depressed

with addition of Nb_2O_5 and the secondary dielectric constant peak was enhanced when sintered above 1280 ^{0}C for higher Nb_2O_5 concentration (≥1.2mol%)**[17]**. Among all the substituted ions at B-site, Mn^{3+} is very good candidate because it has great effects on the electrical and dielectric properties of $BaTiO_3$ **[18]**. Recently many researchers studied the effect of rare-earth doping on $(Ba_{1-x}Ln_x)Zr_{0.2}Ti_{0\cdot8-x/4}O_3$ (Ln = La, Sm, Eu, Dy, Y) ceramics. Chou *et al.* reported the diffuseness of the phase transition and the degree of ferroelectric relaxor behavior are enhanced by the doping. The rare-earth ions with various ionic radii enter the unit cell to substitute for A-site Ba^{2+} ions and inhibit the grain growth **[19]**. Lanthanum concentration has effect on grain growth, as the lanthanum concentration increases, the grain size becomes smaller. $BaTiO_3$ doped with 0.5 mol% of lanthanum sintered for 8 h possesses the highest density. Lanthanum concentration influences on shifting of the Curie temperature to the lower temperatures and increase of dielectric constant **[20]**. BZT is an attractive ceramic due to large change in structural and physical properties after doping on A or B-site. When the Zr content is less than 10mol%, the BZT ceramics shows the normal ferroelectric behavior and dielectric anomalies corresponding to cubic to tetragonal, tetragonal to orthorhombic, and orthorhombic to rhombohedra phase transitions **[21]**. At around 27 mol%, Zr-doped BT ceramics exhibit typical diffuse phase transition behavior, whereas at more than 40 mol% of Zr compositions exhibit typical relaxor-like behavior in which T_c shifts to higher temperature with increase of frequency **[22-24]**. Kumari *at el.* fabricated $(Ba_{0.9575}La_{0.04}X_{0.0025})(Ti_{0.815}Mn_{0.0025}Nb_{0.0025}Zr_{0.18})_{0.99}O_3$ (BLCTMNZ) ceramic material by solid state reaction method and reported ferroelectric behaviour with low dielectric loss **[25]**. According to Jaiban *at el.* BNZ and BNZT ceramics shows the elliptic-shaped hysteresis loops. The rhombohedral phase transition in Ti-added ceramics could enhance the dielectric properties of BNZ prototype material **[26]**.

In this paper we report the $(K_{0.45}Na_{0.45}Li_{0.1}NbO_3)_{1-x}$-$(Ba_{0.96}La_{0.04}Ti_{0.815}Mn_{0.0025}\ Nb_{0.0025}Zr_{0.18}O_3)_x$; where x =0.1, 0.3 0.5, 0.7 and 0.9 lead-free system synthesized by solid-state reaction method. The purpose of this study is to investigate with a special emphasis on the influence of mol% BLTMNZ ($Ba_{0.96}La_{0.04}Ti_{0.815}Mn_{0.0025}\ Nb_{0.0025}Zr_{0.18}O_3$) doping on the structural and various electrical properties of KNLN ($K_{0.45}Na_{0.45}Li_{0.1}NbO_3$).

Experimental

Material synthesis

$(K_{0.45}Na_{0.45}Li_{0.1}NbO_3)_{1-x}$-$(Ba_{0.96}La_{0.04}Ti_{0.815}Mn_{0.0025}Nb_{0.0025}Zr_{0.18}O_3)_x$ ceramics (where x = 0.1, 0.3, 0.5, 0.7 and 0.9) were prepared by using a high temperature solid state reaction technique with analytical-grade metal oxides powders: K_2CO_3 (Aldrich 99.9 %), Na_2CO_3 (Aldrich 99.9 %), Li_2CO_3 (Aldrich 99.9 %), TiO_2 (Aldrich 99.9 %), $BaCO_3$ (Aldrich 99.9 %), ZrO_2 (Aldrich 99.9 %), Nb_2O_5 (Aldrich 99.9 %), MnO_2 (Aldrich 99.9 %), and La_2O_3 (Aldrich 99.9 %). The powders in the suitable stoichiometric ratio of the compositions were weighed and mixed thoroughly in acetone and then dried and calcined at 900 ^{0}C for 4h. The calcined powder was ground in a mortar pestle to obtain fine powder. The calcined fine powder was cold pressed into cylindrical pellets of 10 mm in diameter and 1-2 mm in thickness using a hydraulic press with a pressure of 50 MPa and sintered at a temperature of 950 ^{0}C for 5 hrs in a high temperature muffle furnace. Silver paste was used as electrodes on the top and bottom surfaces of the samples for the electrical measurements.

Characterizations

The crystallite structure of the sintered samples were examined by using X-ray diffraction (XRD) techniques with CuKα radiation (λ = 1.5405 Å) (Rigaku Minifiex, Japan) in a wide range of Bragg angles 2θ ($20^0 \leq 2\theta \leq 60^0$) at a scanning rate of 0.02˚min^{-1}. Dielectric constant, loss tangent, and impedance were determined by use of PSM1734 Impedance analyser at frequencies 1 kHz to 1 MHz; samples were heated from room temperature to 500 ^{0}C.

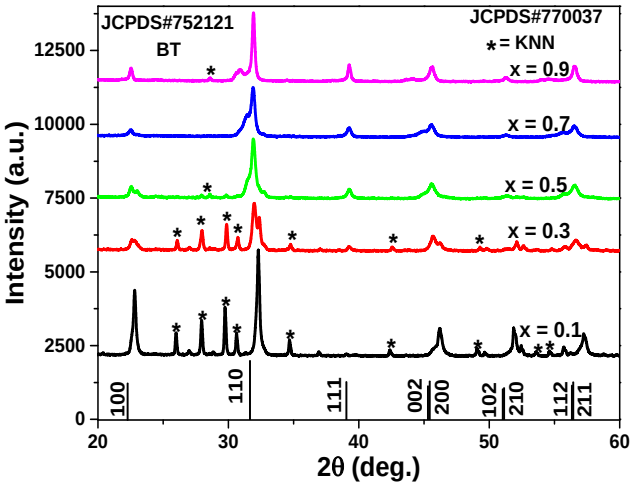

Fig. 1. Room temperature XRD patterns of $(K_{0.45}Na_{0.45}Li_{0.1}NbO_3)_{1-x}$-$(Ba_{0.96}La_{0.04}Ti_{0.815}Mn_{0.0025}\ Nb_{0.0025}Zr_{0.18}O_3)_x$ (where x = 0.1, 0.3, 0.5, 0.7 and 0.9) ceramics.

Results and discussion

Fig. 1 shows the XRD patterns of $(K_{0.45}Na_{0.45}Li_{0.1}NbO_3)_{1-x}$-$(Ba_{0.96}La_{0.04}Ti_{0.815}Mn_{0.0025}\ Nb_{0.0025}Zr_{0.18}O_3)_x$ ceramics at room temperature. BLTMNZ doped KNLN samples with x = 0.1, 0.3, 0.5 have of KNN and BT phase both coexisted **[27]**. Vol. fraction mol% of each phase have been calculated and mentioned in **Table 1**. Whereas other patterns are match with JCPDS#752121 of $BaTiO_3$ sample. As we increase the mol% of BLTMNZ from x = 0.1 to 0.9 the samples have the tetragonal phase. AS we increase the mol% of BLTMNZ $(K_{0.45}Na_{0.45}Li_{0.1}NbO_3)_{1-x}$-$(Ba_{0.96}La_{0.04}Ti_{0.815}Mn_{0.0025}\ Nb_{0.0025}Zr_{0.18}O_3)_x$ with x = 0.7 to 0.9 the different phases are decreases and at 0.7 it gain the pure phase at room temperature. All the reflection peaks were indexed using observed inter-planar spacing d, and lattice parameters of BLTMNZ doped KNLN were determined by using least-squares refinement method. The lattice parameters, d observed values and h k l values of all diffraction lines (reflections) and vol. fraction mol% of the above compounds are shown in **Table 1**. The main peak of all the samples are located at approximately 2θ ≈ 32°, having hkl value <110>. This shows that

$(K_{0.45}Na_{0.45}Li_{0.1}NbO_3)_{1-x}$-$(Ba_{0.96}La_{0.04}Ti_{0.815}Mn_{0.0025}$ $Nb_{0.0025}Zr_{0.18}O_3)_x$ ceramics has pure phase at x = 0.7. Because of the kinetics of the formation, mixtures of $BaTiO_3$ are always obtained as a major phase along with other impurity phases during synthesis. It is also observed that the diffraction peaks shift slightly to a lower angle side as we increase the mol% of BLTMNZ in KNLN.

Table 1. Lattice parameters of $(K_{0.45}Na_{0.45}Li_{0.1}NbO_3)_{1-x}$-$(Ba_{0.96}La_{0.04}Ti_{0.815}Mn_{0.0025}$ $Nb_{0.0025}Zr_{0.18}O_3)_x$ ceramics.

Mol%	Crystal system	Lattice parameter	Vol. mol% *KNN*	*BT*
x = 0.1	Tetragonal	a = 9.7250Å c =12.7534Å	51	49
x = 0.3	Tetragonal	a = 12.3338Å c =11.4424Å	17	83
x = 0.5	Tetragonal	a = 9.6152Å c =11.5509Å	12	88
x = 0.7	Tetragonal	a = 3.9884Å c =4.0001Å	0	100
x = 0.9	Tetragonal	a = 12.6218Å c =11.2634Å	8	92

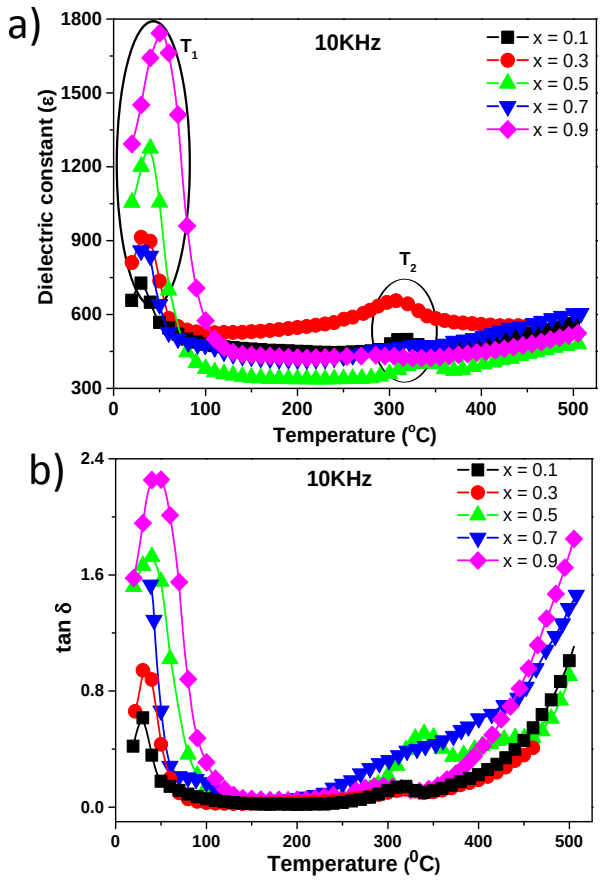

Fig. 2 (a-b). Variation of dielectric constant (ε) and loss tangent (tan δ) of $(K_{0.45}Na_{0.45}Li_{0.1}NbO_3)_{1-x}$-$(Ba_{0.96}La_{0.04}Ti_{0.815}Mn_{0.0025}$ $Nb_{0.0025}Zr_{0.18}O_3)_x$ (where x = 0.1, 0.3, 0.5, 0.7 and 0.9) ceramics with temperature at frequency 10 kHz.

Fig. 2(a) shows the variation of dielectric constant (ε) as a function of temperature of BLTMNZ doped KNLN ceramics at frequency 10 kHz. As in normal ferroelectrics, the dielectric constant of BLTMNZ doped KNLN ceramics with x = 0.7 - 0.9 increases gradually with increasing temperature up to the transition temperature and thereafter it decreases with increasing temperature **[28]**, whereas in case of BLTMNZ doped KNLN with x = 0.1 – 0.5 two peaks are observed; these two peaks are presented due to the presence of different phase of BT and KNN. As we have discussed in **Fig 1,** in all the samples $BaTiO_3$ have the higher value of vol. mol% so they have higher value of dielectric constant. BLTMNZ doped KNLN sample with x = 0.9 shows the maximum value of dielectric constant and Curie temperature T_C. **Fig. 2(b)** shows the variation of dissipation factor (tan δ) as a function of temperature of BLTMNZ doped KNLN ceramics at frequency 10 kHz. Loss tangent initially increases with increasing temperature and after the transition temperature loss tangent decreases with temperature. An important contribution to the losses may occur in bulk ceramics by defects associated with the grain boundaries. This phase transition has diffuse character which can be understood in terms of the inhomogeneous distribution of ions in A and B sites of the ABO_3 perovskite cell. Above the transition temperature it does not follow the Curie-Weiss law as predicted by thermodynamic theory. Value of transition temperature (Curie temperature, T_c), dielectric constants are mentioned in **Table 2** for different compositions at frequency 10 kHz.

Table 2. Details of the physical parameters of $(K_{0.45}Na_{0.45}Li_{0.1}NbO_3)_{1-x}$-$(Ba_{0.96}La_{0.04}Ti_{0.815}Mn_{0.0025}$ $Nb_{0.0025}Zr_{0.18}O_3)_x$ ceramics at 10 kHz.

Mol%	T_1 (°C)	ε_1	T_2 (°C)	ε_2	Diffusivity γ	Activation Energy E_a
x = 0.1	30	727	310	501	1.10	0.65
x = 0.3	35	919	310	655	1.38	0.53
x = 0.5	40	1274	335	404	1.49	0.35
x = 0.7	35	895	-	-	1.13	0.69
x = 0.9	50	1742	-	-	1.82	0.75

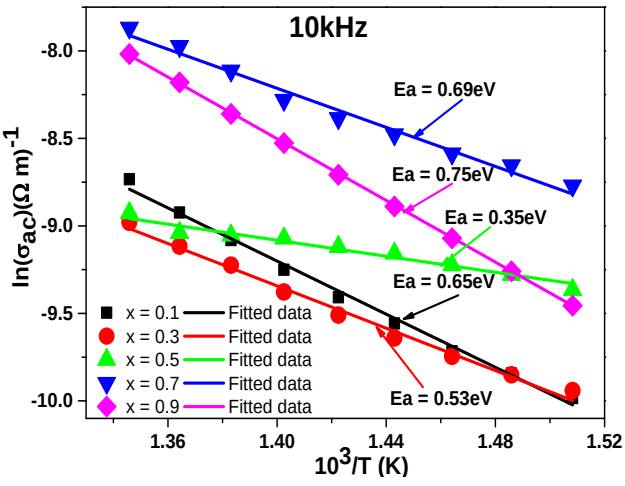

Fig. 3. Variation of ln σ_{ac} $(\Omega\ m)^{-1}$ vs $10^3/T$ of $(K_{0.45}Na_{0.45}Li_{0.1}NbO_3)_{1-x}$-$(Ba_{0.96}La_{0.04}Ti_{0.815}Mn_{0.0025}$ $Nb_{0.0025}Zr_{0.18}O_3)_x$ (where x = 0.1, 0.3, 0.5, 0.7 and 0.9) ceramics for frequency 10 kHz.

Fig. 3 shows the variation of log σ_{ac} $(\Omega cm)^{-1}$ vs. $10^3/T$ (K^{-1}) of BLTMNZ doped KNLN ceramic at frequency 10

kHz in the higher temperature range. The ac electrical conductivity was calculated from the impedance data collected with LCR meter using the formula $\sigma = \omega\varepsilon\varepsilon_o \tan\delta$, where ε is the vacuum dielectric constant, ω is the angular frequency and k_B is the Boltzmann constant. As the temperature increases the ac conductivity also increases. This may be due to ionic solids having a limited number of mobile ions being trapped in relatively stable potential wells during their motion through the solid. Due to a rise in temperature the donor cations are taking a major part in the conduction process. The donors have created a level (i.e. band-donor level), which is much nearer to the conduction band. Therefore, only a small amount of energy is required to activate the donors. In addition to this, a slight change in stoichiometry in multi-metal complex oxides causes the creation of large number of donors or acceptors, which creates donor or acceptors like states in the vicinity of conduction or valance bands. These donors or acceptors may also be activated with small energy **[29]**. The value of activation energy was calculated in the paraelectric region from the slope of $\ln(\sigma_{ac})$ vs $10^3/T$ using the conductivity relation $\sigma = \sigma_o \exp(-E_a/k_BT)$ and value of activation energy indexed in **Table 2**.

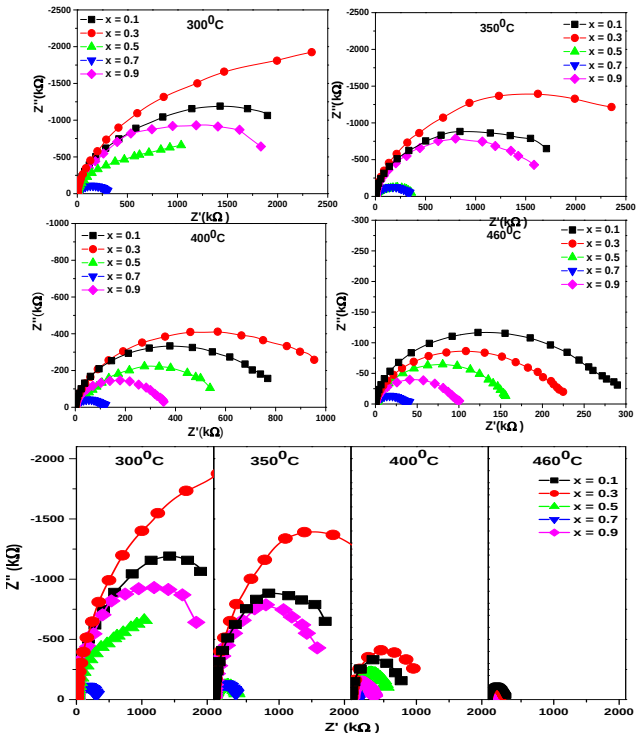

Fig. 4. Variation of real and imaginary part of impedance at different temperatures of $(K_{0.45}Na_{0.45}Li_{0.1}NbO_3)_{1-x}$-$(Ba_{0.96}La_{0.04}Ti_{0.815}Mn_{0.0025}Nb_{0.0025}Zr_{0.18}O_3)_x$ (where x = 0.1, 0.3, 0.5, 0.7 and 0.9) ceramics.

The electrical properties of BLTMNZ doped KNLN materials were investigated by a complex impedance spectroscopy (CIS) technique. It is an important tool to analyze the electrical properties of a polycrystalline material in view of its capability of correlating the sample electrical behavior to its microstructure. The use of function Z* and Y* is particularly appropriate for the resistive and/or conductive analysis where the long-range conduction dominates, whereas the ε* and M* functions are suitable when localized relaxation dominates. So the plotting of ac data in terms of impedance, electric modulus, and dielectric permittivity simultaneously gives a complete assignment of all the physical processes taking place in the material. **Fig. 4** shows the temperature-dependent spectra (Nyquist plot) of $(K_{0.45}Na_{0.45}Li_{0.1}NbO_3)_{1-x}$-$(Ba_{0.96}La_{0.04}Ti_{0.815}Mn_{0.0025}Nb_{0.0025}Zr_{0.18}O_3)_x$ ceramics for x = 0.1, 0.3, 0.5, 0.7 and 0.9 ceramic material. By impedance spectrum we got the semicircle arcs. The nature of variation of the arcs with temperature and frequency provides various clues of the materials. The impedance spectra are characterized by the appearance of a single semicircle arc and the intercept of the semicircle arc with the real axis (Z′) gives us an estimate of the bulk resistance (R_b) of the material. It is clear from the figure semicircle arcs decreases with the increasing temperature. Therefore the bulk resistance of the material decreases with increasing temperature showing a typical semiconducting property, i.e. negative temperature coefficient of resistance (NTCR) behavior.

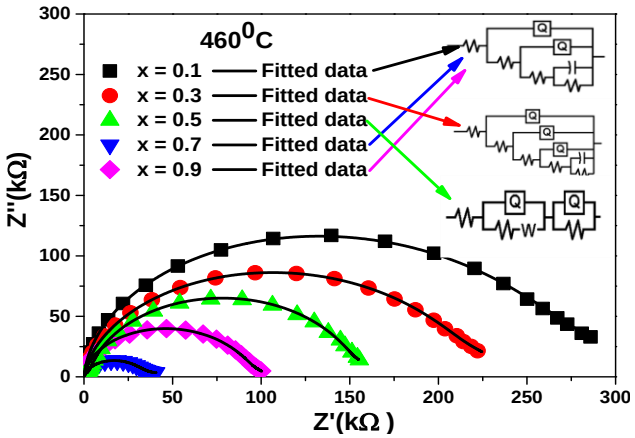

Fig. 5. Fitting of Cole-cole plot at 460°C of $(K_{0.45}Na_{0.45}Li_{0.1}NbO_3)_{1-x}$-$(Ba_{0.96}La_{0.04}Ti_{0.815}Mn_{0.0025}\ Nb_{0.0025}Zr_{0.18}O_3)_x$ (where x = 0.1, 0.3, 0.5, 0.7 and 0.9) ceramics.

It is observed that with the increase in temperature the slope of the lines decrease and the lines bend towards real (Z′) axis above 350 ^{0}C; a semicircle could be traced, indicating the increase in conductivity of the sample. It can also be observed that the peak maxima of the plots decrease and the frequency for the maximum shifts to higher values with the increase in temperature. It can be noticed that the complex impedance plots are not represented by full semicircle, rather the semicircle arc is depressed and the centre of the arc lies below the real (Z′) axis suggesting the relaxation to be of polydispersive non-Debye type in samples. This may be due to the presence of distributed elements in the material electrode system **[30, 31]. Fig. 5** shows equivalent circuits is being used to provide a complete picture of the system and establish the structural property relationship of the materials. Comparison of complex impedance plots (symbols) with fitted data (lines) using commercially available software ZSimpwin Version 2 **[32]** has been given in the **Fig. 5**. To model the non-Debye response, constant phase element (CPE) is used in addition to resistors and capacitors. Here it has also been clearly observed from the Nyquist plots that the influence of grain size on the inter grain resistivity increases with decreasing grain size.

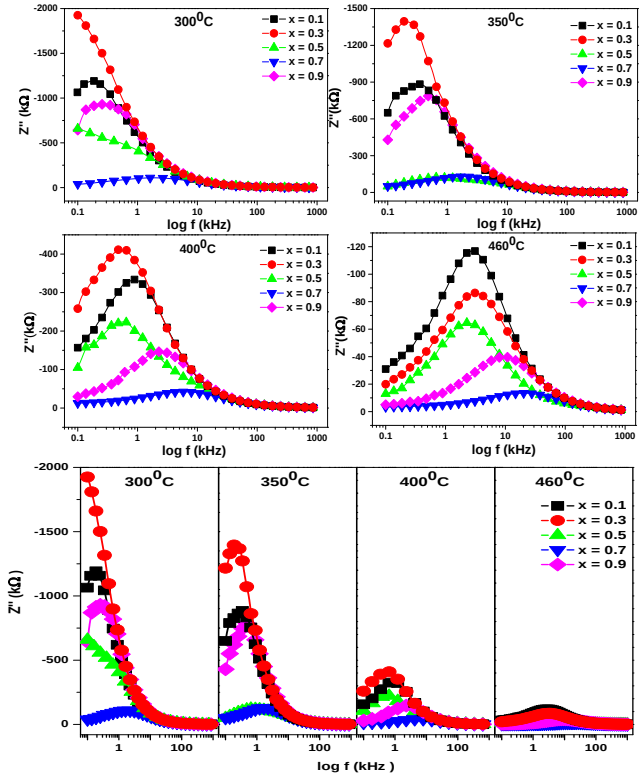

Fig. 6. Variation of imaginary part (Z″) of impedance with frequency at different temperatures of $(K_{0.45}Na_{0.45}Li_{0.1}NbO_3)_{1-x}$-$(Ba_{0.96}La_{0.04}Ti_{0.815}Mn_{0.0025}\ Nb_{0.0025}Zr_{0.18}O_3)_x$ (where x = 0.1, 0.3, 0.5, 0.7 and 0.9) ceramics.

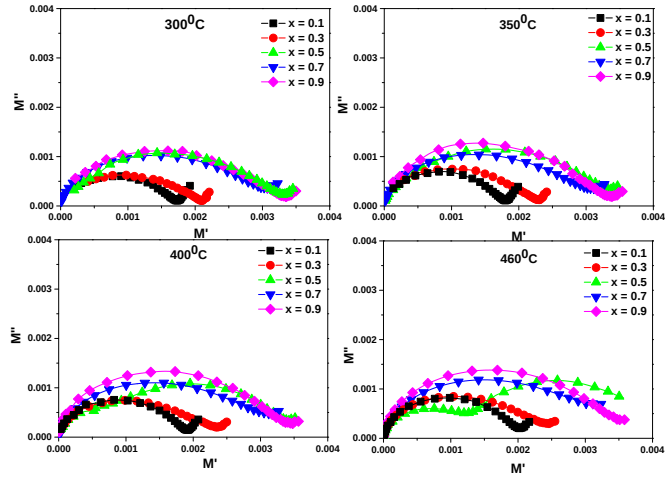

Fig. 7. Variation of real and imaginary part of modulus at different temperatures of $(K_{0.45}Na_{0.45}Li_{0.1}NbO_3)_{1-x}$-$(Ba_{0.96}La_{0.04}Ti_{0.815}Mn_{0.0025}Nb_{0.0025}Zr_{0.18}O_3)_x$ (where x = 0.1, 0.3, 0.5, 0.7 and 0.9) ceramics.

Fig. 6 presents the variation of imaginary part of impedance (Z″) as a function of frequency at different set of temperatures. With the increase of frequency, imaginary part of impedance (Z″) increases with increase of frequency and then decreases after a particular point. At higher frequency side all the curves are merged. As the temperature increases, the peak in Z″ versus frequency plot becomes more prominent. The peak shifts towards higher frequency side with increasing temperature showing that the resistance of the bulk material is decreasing. Also, the magnitude of Z″ decreases with increasing temperature. This would imply that dielectric relaxation is temperature dependent, and there is apparently not a single relaxation time.

Electrical response of the materials can also be analyzed through complex electric modulus formalism, which provides an alternative approach based on polarization analysis. Complex electric formalism gives the inhomogeneous nature of the polycrystalline ceramic, which can be probed into bulk and grain boundary effects. The complex electric modulus spectrum M′ versus M″ is shown in **Fig. 7** for $(K_{0.45}Na_{0.45}Li_{0.1}NbO_3)_{1-x}$-$(Ba_{0.96}La_{0.04}Ti_{0.815}Mn_{0.0025}\ Nb_{0.0025}Zr_{0.18}O_3)_x$ ceramics for x = 0.1, 0.3, 0.5, 0.7 and 0.9 at different temperatures. The patterns are characterized by the presence of little asymmetric and depressed semicircle arcs whose centre does not lie on M′ axis. The behaviour of electric modulus spectrum is suggestive of the temperature dependent hopping type of mechanism for electric conduction (charge transport) in the system and non-Debye type dielectric relaxation. In a relaxation system, one can determine the probable relaxation time (s) from the position of the loss peak in the Z″ as well as M″ vs. log f plots according to the relation: $\tau = 1/\omega = 1/2\pi f$ (f is the relaxation frequency). Above 400 ^{0}C temperature BLTMNZ doped KNLN at x = 0.5 have double semicircle arc; there is a possibility to coexistence of both systems in this sample.

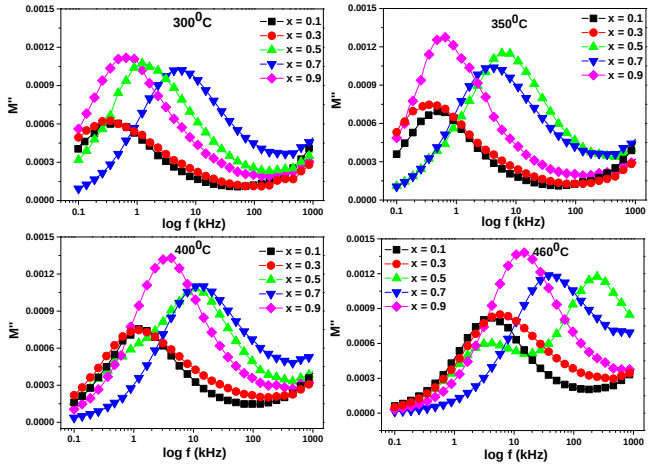

Fig. 8. Variation of imaginary part (M″) of modulus with frequency at different temperatures of $(K_{0.45}Na_{0.45}Li_{0.1}NbO_3)_{1-x}$-$(Ba_{0.96}La_{0.04}Ti_{0.815}Mn_{0.0025}\ Nb_{0.0025}Zr_{0.18}O_3)_x$ (where x = 0.1, 0.3, 0.5, 0.7 and 0.9) ceramics.

Fig. 8 shows the variation of imaginary part of modulus (M″) with frequency at different temperatures for different compositions. By these graphs we found that the position of the peak M''_{max} shifted to higher frequencies as the temperature was increased. The frequency region below peak maximum M″ determines the range in which charge carriers are mobile on long distances. At frequency above peak maximum, the carriers are confined to potential wells, being mobile on short distances. The peaks are asymmetric and broader than the ideal Debye curve. The frequency range where the peaks occur, which indicate the transition from long range to short range mobility **[33, 34]**.

Fig. 9 shows the normalized plot of Z''/Z''_{max} vs. log (f/f_{max}) at different temperatures for different compositions

of BLTMNZ doped KNLN ceramics. The normalized plot overlaps on a single master curve at different temperatures i.e. same shape and pattern in the peak position with slight variation in full width at half maximum FWHM with rise in temperature. Thus the dielectric processes occurring in the material can be investigated via master admittance plot **[35]**. The value of FWHM evaluated from the normalized spectrum is greater than log $\frac{2+\sqrt{3}}{2-\sqrt{3}}$, and this indicates the non-Debye type behavior which is well supported by complex admittance plot also.

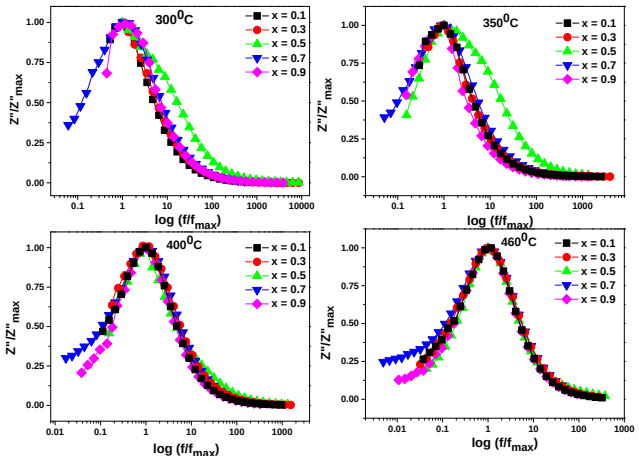

Fig. 9. Impedance scaling behavior of compounds in the master curves of $(K_{0.45}Na_{0.45}Li_{0.1}NbO_3)_{1-x}$-$(Ba_{0.96}La_{0.04}Ti_{0.815}Mn_{0.0025}Nb_{0.0025}Zr_{0.18}O_3)_x$ (where x = 0.1, 0.3, 0.5, 0.7 and 0.9) ceramics.

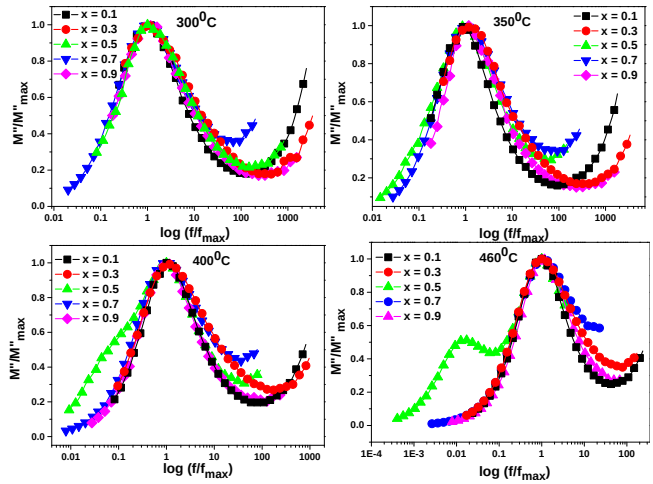

Fig. 10. Modulus scaling behavior of compounds in the master curves of $(K_{0.45}Na_{0.45}Li_{0.1}NbO_3)_{1-x}$-$(Ba_{0.96}La_{0.04}Ti_{0.815}Mn_{0.0025}Nb_{0.0025}Zr_{0.18}O_3)_x$ (where x = 0.1, 0.3, 0.5, 0.7 and 0.9) ceramics.

Fig. 10 shows the modulus master curve of the sample at various temperatures. The capacitance values are calculated at the maximum frequency (f_{max}) using the relation $M'' = \varepsilon_0/2C$. The modulus peak maximum shifts to higher frequencies as temperature increases but the shape and full-width at half-maximum (FWHM) of M''/M''_{max} vs. f/f_{max} do not change in the temperature range 300 – 460 ^{0}C. The overlap of all the curves at different temperatures at a single point indicates that the dynamical processes are nearly temperature independent. It is observed from the fig. that the M''/M''_{max} curves are not symmetric, implying a non-exponential behavior of the conductivity relaxation. The full width at half maximum (FWHM) of M''/M''_{max} vs. f/f_{max} is wider than the breath of a Debye peak, which shows the presence of non-Debye type of relaxation phenomenon **[36]**.

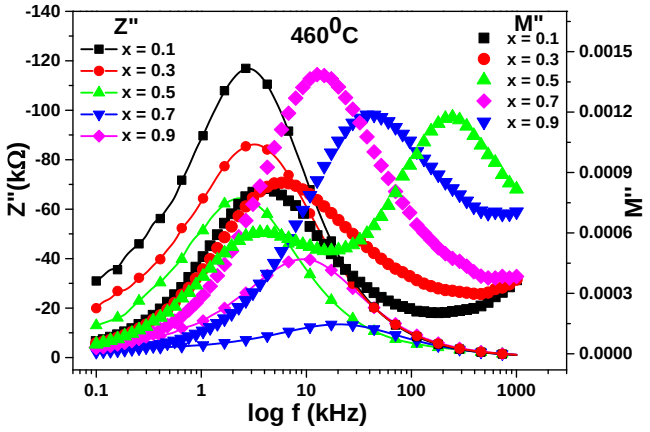

Fig. 11. Variation of Z″ and M″ with frequency at 460°C temperature of $(K_{0.45}Na_{0.45}Li_{0.1}NbO_3)_{1-x}$-$(Ba_{0.96}La_{0.04}Ti_{0.815}Mn_{0.0025}Nb_{0.0025}Zr_{0.18}O_3)_x$ (where x = 0.1, 0.3, 0.5, 0.7 and 0.9) ceramics.

Fig. 11 compares the frequency-dependent behavior of M″ and Z″ for the sample at high temperature (460 ^{0}C). It was found that there is a wide gap between M″ and Z″ peaks showing the departure from Debye type of behaviours. The Z″ peaks are asymmetric at lower frequency side while M″ peak are asymmetric on the higher frequency side. In the entire range of observed temperature no overlapping temperature could be found, indicating that the samples have component both from long range conductivity and localized relaxation. BLTMNZ doped KNLN at x = 0.1 have maximum value of Z″; whereas BLTMNZ doped KNLN at x = 0.9 have maximum value of M″.

Conclusion

Dielectric properties of $(K_{0.45}Na_{0.45}Li_{0.1}NbO_3)_{1-x}$-$(Ba_{0.96}La_{0.04}Ti_{0.815}Mn_{0.0025}Nb_{0.0025}Zr_{0.18}O_3)_x$ ceramics (Where x = 0.1, 0.3, 0.5, 0.7 and 0.9) have been investigated by using Impedance Spectroscopy (IS) over a wide range of temperature (30 - 460 ^{0}C) under different frequency range (100Hz-1MHz). BLTMNZ doped KNLN at x = 0.7 have single pervoskite phase with tetragonal structure at room temperature; which indicate the maximum solubility of both these ceramics. BLTMNZ doped KNLN sample with x = 0.9 have maximum value of transition temperature and diffusivity as compare to other samples. The compounds showed dielectric relaxation, which is found to be of non-Debye type and the relaxation frequency shifted to higher side with the increase of temperature. The Nyquist plot and conductivity studies showed the NTCR behaviour of ceramics. Study of ac conductivity confirms that BLTMNZ doped KNLN ceramics follows the Arrhenius law.

Author contributions
Authors are grateful to the Defence Research and Development Organization (DRDO), Govt. of India, for financial support under the research project ERIP/ER/1303129/M/01/1564.

Reference

1. Ringgaard, E.; Wurlitzer, T. *Journal of the European Ceramic Society* **2005**, *25*, 2701. **DOI:** 10.1155/2014/365391
2. Ichiki, M.; Zhang, L.; Tanaka, M.; Maeda, R. *Journal of the European Ceramic Society* **2004**, *24*, 1693. **DOI:** 10.1016/s0955-2219(03)00475-8
3. Saito, Y.; Takao, H.; Tani, T.; Nonoyama, T.; Takatori, K.; Homma, T.; Nagaya, T.; Nakamura, M. *Nature* **2004**, *432*, 84. **DOI:** 10.1038/nature03028
4. Smeltere, I.; Antonova, M.; Kalvane, A.; Grigs, O.; Livinsh, M. *Materials Science* **2011**, *17*, 62. **DOI:** 10.5755/j01.ms.17.1.251
5. Liu, Z.; Fan, H.; Long, C. *Journal of materials science* **2014**, *49*, 8107. **DOI:** 10.1007/s10853-014-8518-3
6. Li, J. F.; Wang, K.; Zhu, F. Y.; Cheng, L. Q.; Yao, F. Z. *Journal of the American Ceramic Society* **2013**, *96*, 3677. **DOI:** 10.1111/jace.12715
7. Shirane, G.; Newnham, R.; Pepinsky, R. *Physical Review* **1954**, *96*, 581. **DOI:** 10.1103/PhysRev.96.581
8. Wang, K.; Li, J. F. *Advanced Functional Materials* **2010**, *20*, 1924. **DOI:** 10.1002/adfm.201000284
9. Hollenstein, E.; Damjanovic, D.; Setter, N. *Journal of the European Ceramic Society* **2007**, 27, 4093. **DOI:** 10.1016/j.jeurceramsoc.2007.02.100
10. Du, H.; Liu, D.; Tang, F.; Zhu, D.; Zhou, W.; Qu, S. *Journal of the American Ceramic Society* **2007**, *90*, 2824. **DOI:** 10.1111/j.1551-2916.2007.01846
11. Du, H.; Luo, F.; Qu, S.; Pei, Z.; Zhu, D.; Zhou, W. *Journal of Applied Physics* **2007**, *102*, 054102. **DOI:** 10.1063/1.2775997
12. Park, J.-H. *TRANSACTIONS ON ELECTRICAL AND ELECTRONIC MATERIALS* **2012**, *13*, 297. **DOI:**10.4313/TEEM.2012.13.6.297
13. Cai, W.; Fu, C.; Gao, J.; Zhao, C. *Advances in Applied Ceramics* **2011**, *110*, 181. **DOI:** 10.1179/1743676110Y.0000000019
14. Mitic, V. V.; Nikolic, Z. S.; Pavlovic, V. B.; Paunovic, V.; Miljkovic, M.; Jordovic, B.; Zivkovic, L. *Journal of the American Ceramic Society* **2010**, *93*, 132. **DOI:** 10.1111/j.1551-2916.2009.03309
15. Om, P.; Kumar, D.; Dwivedi, R. K.; Srivastava, K. K.; Singh, P.; Singh, S. *Journal of Materials Science* **2007**, *42*, 5490. **DOI:** 10.1007/s10853-006-0985-8
16. Lu, D.-Y.; Toda, M.; Sugano, M. *Journal of the American Ceramic Society* **2006**, *89*, 3112. **DOI:** 10.1111/j.1551-2916.2006.00893
17. Yuan, Y.; Zhang, S.; Zhou, X.; Tang, B. *Journal of materials science* **2009**, *44*, 3751. **DOI:**10.1007/s10853-009-3502-z
18. Cha, S. H.; Han, Y. H. *Journal of Applied Physics* **2006**, *100*, 104102. **DOI:** 10.1063/1.2386924
19. Chou, X.; Zhai, J.; Jiang, H.; Yao, X. *Journal of Applied Physics* **2007**, *102*, 084106. **DOI:** 10.1063/1.2799081
20. Vijatović, M.; Stojanović, B.; Bobić, J.; Ramoska, T.; Bowen, P. *Ceramics International* **2010**, *36*, 1817. **DOI:** 10.1016/j.ceramint.2010.03.010
21. Zaghete, M. A.; Simões, A. Z.; Longo, E.; Moura, F.; Varela, J. A., *Influence of Dopants, Temperature and Atmosphere of Sintered on the Microstructure and Behavior of Lead Free Ceramics*. INTECH Open Access Publisher: **2011**. **DOI:** 10.5772/19543
22. Nanakorn, N.; Jalupoom, P.; Vaneesorn, N.; Thanaboonsombut, A. *Ceramics International* **2008**, *34*, 779. **DOI:** 10.1016/j.ceramint.2007.09.024
23. Badapanda, T.; Rout, S.; Cavalcante, L.; Sczancoski, J.; Panigrahi, S.; Sinha, T. P.; Longo, E. *Materials Chemistry and Physics* **2010**, *121*, 147. **DOI:** 10.1016/j.matchemphys.2010.01.008
24. Moura, F.; Simoes, A.; Stojanovic, B.; Zaghete, M.; Longo, E.; Varela, J. *Journal of Alloys and Compounds* **2008**, *462*, 129. **DOI:** 10.1016/j.jallcom.2007.07.077
25. Kumari, P.; Rai, R.; Kholkin, A. L.; Tiwari, A. *Advanced Materials Letters* **2014**, *5*, 255. **DOI:** 10.5185/amlett.2013.10547
26. Jaiban, P.; Jiansirisomboon, S.; Watcharapasorn, A.; Yimnirun, R.; Guo, R.; Bhalla, A. S. *Ceramics International* **2013**, *39*, S81. **DOI:** 10.1016/j.ceramint.2012.10.039
27. Shimojo, Y.; Wang, R.; Sekiya, T.; Matsuzaki, K. *Journal of the Korean Physical Society* **2005**, *46*, 48.
28. Gao, F.; Dong, X.; Mao, C.; Liu, W.; Zhang, H.; Yang, L.; Cao, F.; Wang, G. *Journal of the American Ceramic Society* **2011**, *94*, 4382. **DOI:** 10.1111/j.1551-2916.2011.04731.x
29. Shu, L.; Wei, X.; Jin, L.; Li, Y.; Wang, H.; Yao, X. *Applied Physics Letters* **2013**, *102*, 152904. **DOI:** 10.1063/1.4802450
30. Mcdonald, J. R. *A Wiley-Interscience Publication, John Wiley & Sons, New York* **1987**.
31. Sharma, D. K.; Kumar, R.; Rai, R.; Sharma, S.; Kholkin, A. L. *Journal of Advanced Dielectrics* **2012**, *2*. **DOI:** 10.1142/S2010135X12500026
32. Yeum, B. *Ann Arbor, MI: EChem Software* **2001**.
33. Rai, R.; Coondoo, I.; Rani, R.; Bdikin, I.; Sharma, S.; Kholkin, A. L. *Current Applied Physics* **2013**, *13*, 430. **DOI:** 10.1016/j.cap.2012.09.009
34. Shukla, A.; Choudhary, R.; Thakur, A. *Journal of Physics and Chemistry of Solids* **2009**, *70*, 1401. **DOI:** 10.1016/j.jpcs.2009.08.015
35. Shukla, A.; Choudhary, R.; Thakur, A. *Journal of Materials Science: Materials in Electronics* **2009**, *20*, 745. **DOI:** 10.1007/s10854-008-9797-8
36. Padmasree, K.; Kanchan, D.; Kulkarni, A. *Solid State Ionics* **2006**, *177*, 475. **DOI:** 10.1016/j.ssi.2005.12.019

